Journal of Applied Geophysics 241 (2025) 105826

Contents lists available at ScienceDirect

Journal of Applied Geophysics

journal homepage: www.elsevier.com/locate/jappgeo

A comparison and combination of stable platform and strapdown airborne gravimeters

Felix Johann [a,*], Hannes Eisermann [b], Graeme Eagles [b]

[a] Technical University of Darmstadt, Physical and Satellite Geodesy, Franziska-Braun-Str. 7, 64287 Darmstadt, Germany
[b] Alfred Wegener Institute for Polar and Marine Research, Am Alten Hafen 26, 27568 Bremerhaven, Germany

ARTICLE INFO

Keywords:
Airborne gravimetry
IMU
GNSS
Radar
Antarctica
Combination

ABSTRACT

Airborne gravimetry is an important technique for gravity field determination and sub-surface interpretations in geophysics and exploration. Traditionally, stable platform gravimeters were used, which maintained the gravity sensor's alignment with the local vertical. Recent advancements resulted in an increased utilisation of strapdown gravimeters. This study compares the performance of a GT-2A stable platform gravimeter and an iMAR iNAV-RQH-1003 strapdown gravimeter, which were operated simultaneously in an airborne campaign at East Antarctica. Furthermore, novel combination approaches for the individual gravimeter solutions are presented and assessed. The strapdown gravimeter demonstrated superior overall precision (1.71 mGal without crossover adjustment, 1 mGal = 10^{-5} m/s^2), lower high-frequency noise and lower line-to-line biases compared to the GT-2A (2.40 mGal) but was susceptible to significant flight-to-flight biases. However, the elimination of these flight biases is possible through the estimation of a single bias per flight via crossover adjustment. Moreover, the benefits of strapdown technology, including reduced space, weight, and operational requirements, contribute to the growing preference for strapdown over stable platform gravimeters. All combination approaches yielded improved solutions compared to the single gravimeter results, despite the different noise levels of the single gravimeter results. After crossover adjustment, a precision of 1.0 mGal was obtained. This highlights the potential for enhanced gravity field determination when using two or more high-precision gravimeters, provided that their frequency-dependent noise characteristics are considered appropriately.

1. Introduction

1.1. Gravimetry and its applications

The field of gravimetry encompasses the determination of the gravity field, a discipline with applications across several domains, including geodesy, geophysics, and exploration. Since gravity at and above ground depends on sub-surface densities, gravimetry is a valuable technique for sub-surface interpretations. Cavities or low-density materials, such as mineral oil, coal, or clay, induce a lower gravity than solid rocks. Borders of sub-surface materials can be identified using gravity anomaly maps.

On land, topography can be modelled using radar or LIDAR (light detection and ranging) techniques, among others (Wilson, 2012). At sea, in terms of accuracy, shipborne sonar is the optimal technique for bathymetric mapping at depths ranging from medium to the deepest (Dierssen and Theberge, 2014). Alternatively, satellite altimetry can be used featuring limited accuracy but global coverage. With this technique, bathymetry is modelled in a way that it explains gravity-related variations in the primary altimetry result, the sea surface height variations.

The bathymetry beneath shelf ice is inaccessible to ships and radar is much more effective in penetrating ice than water, particularly saline water (Moorman and Michel, 1997). Alternative methods for bathymetry determination such as seismic surveying can be employed but these are time-consuming and expensive (Tankersley, 2023). For this reason, sub-shelf regions with undetermined bathymetry still exist (Eisermann et al., 2024). Airborne gravimetry enables the efficient modelling of sub-shelf bathymetry based on assumed densities of bedrock, sea water, and shelf ice.

Mobile gravimeters measure the so-called specific force, which is the force per unit mass, i.e. the acceleration, that prevents an object from being in free fall. For a moving object in the Earth's gravity field, the specific force $\boldsymbol{f}^i$ is the difference between the kinematic acceleration $\ddot{\boldsymbol{r}}^i$

* Corresponding author.
E-mail address: johann@psg.tu-darmstadt.de (F. Johann).

https://doi.org/10.1016/j.jappgeo.2025.105826
Received 1 November 2024; Received in revised form 12 February 2025; Accepted 11 June 2025
Available online 12 June 2025

due to the vehicle movement and gravity acceleration $\boldsymbol{g}^i$. Therefore, to obtain gravity, the observed specific force must be subtracted from the kinematic acceleration as

$$\boldsymbol{f}^i = \ddot{\boldsymbol{r}}^i - \boldsymbol{g}^i \Leftrightarrow \boldsymbol{g}^i = \ddot{\boldsymbol{r}}^i - \boldsymbol{f}^i \quad (1)$$

with all quantities noted in an inertial frame *i*. The kinematic acceleration is typically determined using Global Navigation Satellite Systems (GNSS) observations. Airborne gravimetry results are usually expressed in terms of gravity disturbance, defined as the discrepancy between the observed gravity and the normal gravity of the Earth, i.e. the gravity of the Earth approximated as a rotational ellipsoid of homogeneous density. Both quantities are given at the point of observation. Gravity disturbance is predominantly influenced by topography and crustal density variations.

1.2. Recent developments in airborne gravimetry

In the decades following the initial airborne gravimetry tests conducted in the 1950s (Nabighian et al., 2005), horizontally stabilised platforms were used to ensure that the single sensitive axis of the gravimeters aligned with the local vertical. An alternative approach to such gravimeters employs inertial measurement units (IMUs) "strapped down" to the aircraft body. As an IMU contains triads of accelerometers and gyroscopes, the observed 3-D accelerations potentially enable 3-D gravity vector determination. Furthermore, the use of strapdown gravimeters results in reduced weight, space, maintenance, and operational requirements. After a first flight in 1995 (Wei and Schwarz, 1998), subsequent side-by-side comparisons demonstrated that strapdown gravimeters exhibited an accuracy on par to that of their counterparts (Glennie et al., 2000; Jensen et al., 2019; Studinger et al., 2008). The strapdown gravimeters were found to be more robust in draped (terrain following) flight mode and during turbulent flight conditions (Förste et al., 2020; Jensen et al., 2019; Petrovic et al., 2015; Studinger et al., 2008). Furthermore, less data gaps arise due to malfunctions, and initialisation time on new flight lines (Jensen et al., 2019; Johann, 2023; Studinger et al., 2008). In the related field of shipborne gravimetry, Yuan et al. (2020) described a side-by-side comparison of four stable-platform gravimeters CHZ-II, ZL11, GT-2M, LaCoste & Romberg (LCR) S-type, and two strapdown gravimeters SAG-2M, SAG-WZ. For all gravimeters except for the LCR, they report similar gravity precision, with the best results obtained using the stable-platform GT-2M and the strapdown SAG-2M.

Significant enhancements in the strapdown results were achieved following the elimination of the majority of thermally induced accelerometer errors through thermal calibration (Becker, 2016; Becker et al., 2015b) or thermal stabilisation (Jensen et al., 2019; Johann et al., 2020; Simav et al., 2020). A magnetic field correction was defined, resulting in significant improvements for accelerometers using capacitive pendulum displacement acquisition, exemplified by the Honeywell Q-Flex accelerometer (Johann et al., 2021). An overview on strapdown gravimeter types and recent trends in strapdown gravimetry, like the installation of gravimeters in Unmanned Aerial Vehicles (UAVs), can be found in Peshekhonov et al. (2022).

Notable long-term drifts are suspected to remain in strapdown gravimetry results (Glennie et al., 2000), even after thermal correction (Jensen, 2018). If a stable platform and a strapdown gravimeter are run side-by-side, their differing properties may be combined to enhance the overall result. In the following, the term "stability" is used to qualitatively describe the level of sensor errors. Assuming better long-term stability, i.e. low sensor drifts over hours up to some days, of a stable platform device and good short-term stability, i.e. low sensor noise and short-term sensor drifts, of a strapdown gravimeter, Jensen et al. (2019) proposed the replacement of the flight lines' mean values of the (thermally stabilised) strapdown results by the corresponding means of the stable platform gravimeter. For a spring-type ZLS Dynamic gravimeter (D-Type) and an iMAR iNAT-RQH strapdown IMU, they reported a precision improvement of 20 % and 56 % compared to the single strapdown and stable platform precision, respectively. For the same IMU without temperature stabilisation, Jensen et al. (2017) merged the strapdown results with those of a LCR S-type by replacing the bias and linear trend per flight line, resulting in precision improvements of 47 % and 41 % for the strapdown and LCR gravimeter, respectively. In an alternative approach, Johann (2023) filtered the shipborne stable platform results of a Chekan-AM and the strapdown results of an iMAR iNAV-RQH with complementary low and high pass filters, respectively, and merged the remaining signals. The combined results aggregated the most desirable properties of both devices, namely the high long-term stability of the Chekan-AM, and the complete trajectory coverage and robustness against harsh sea conditions of the iNAV.

1.3. Study outline

This paper compares the stable platform gravimeter GT-2A and the strapdown gravimeter iMAR iNAV-RQH-1003 using an airborne campaign conducted in Antarctica as an example. Section 2 will introduce the campaign, the two gravimeters, the basics of the applied processing strategies, and the quality evaluation approach. Furthermore, methods for combining both datasets will be developed. In Section 3, the results of each gravimeter will be presented and compared. At the example of a flight line over grounded ice, the plausibility of the results will be verified by comparison with the local topography. Section 4 will discuss the observed advantages and disadvantages of both gravimeters and will assess the combination strategies.

2. Campaign introduction and methods

In December 2022 and January 2023, the Alfred Wegener Institute (AWI) conducted an airborne campaign, called "RIISERBATHY", at the Riiser Larsen shelf ice in Queen Maud Land, East Antarctica. In a collaboration with the German Federal Agency for Geosciences and Natural Resources (BGR) and the Technical University of Darmstadt (TUDa), magnetic, gravity, and ice penetrating radar data were collected to expand knowledge about the region's ice-ocean interactions and its glacial and geodynamical history. Ten survey flights with a total line length exceeding 12,000 km at an average altitude of 1 km and a median line velocity of 76 m/s were conducted using the polar aircraft "Polar 5" of the Basler BT-67 type (Fig. 1), operated from the German Neumayer-III station (NM-III). The present paper will focus on gravity data acquired by two gravimeters simultaneously.

This includes a strapdown gravimeter of the iMAR iNAV-RQH-1003 ("iNAV") type, owned by the TUDa, and a stable platform gravimeter of the GT-2A type by Canadian Micro Gravity (CMG), owned by the AWI (Fig. 2). Both gravimeters have previously been installed in this aircraft type on several occasions but have not been operated at the same time yet. Under optimal conditions during test flights near Bremerhaven, Germany in 2014 and 2021, the individual Root Mean Square Errors (RMSE) of both devices were approximately 0.5 mGal (1 mGal = 10^{-5}

Fig. 1. Polar 5 aircraft at Bremen, Germany (Johann, 2023).

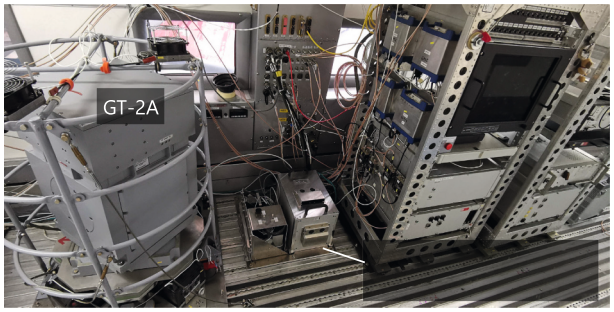

Fig. 2. Gravimeters GT-2A and iMAR iNAV-RQH installed in the Polar 5 aircraft cabin (Johann, 2023).

m/s^2) (Eisermann, 2021; supporting information in Eisermann et al., 2020; Johann, 2023). Above Chilean glaciers with a highly variable gravity field, a crossover RMSE of 1.5 mGal was obtained with the iNAV, although straight flight lines were lacking (Johann, 2023). Using an aircraft of the same type in Antarctica, another research group reported a precision of 1.5 mGal when comparing the results of another GT-2A and a strapdown gravimeter SGA02 (Cao et al., 2023).

Due to noise with frequencies several orders of magnitude higher than the desired output gravity disturbance signal, rigid low-pass filtering is required in airborne gravimetry (Forsberg and Olesen, 2010). In the scope of this work, the same low-pass filter is applied to the gravity disturbance of both gravimeters. The filter was designed as a finite impulse response (FIR) filter using the window method with a fixed filter order of 1024 and a Hamming window. A filter length of 130 s was selected, corresponding to the inverse of the −6 dB cut-off frequency. Fig. 3 visualises the magnitude and impulse response of the filter. The choice of the filter length will be further evaluated in Section 3.2. The filter is successively applied in forward and backward directions.

Before and after each flight, a base reading was conducted during the aircraft's stationary phase. This serves two purposes: firstly, the initial and final attitudes are determined in an alignment algorithm; secondly, the periods are used to anchor the results to an external gravity disturbance reference ("end-matching"), which is a requirement for all relative gravimeters. Between the base readings, linear sensor drift is assumed. Consequently, all subsequent results will be presented with the airport biases and linear drifts already removed for each flight. Measurements with a portable terrestrial LCR gravity meter close to the NM-III runway and at a point of known absolute gravity at the Norwegian Troll station (Kazama et al., 2019) were used as a reference for both gravity data sets.

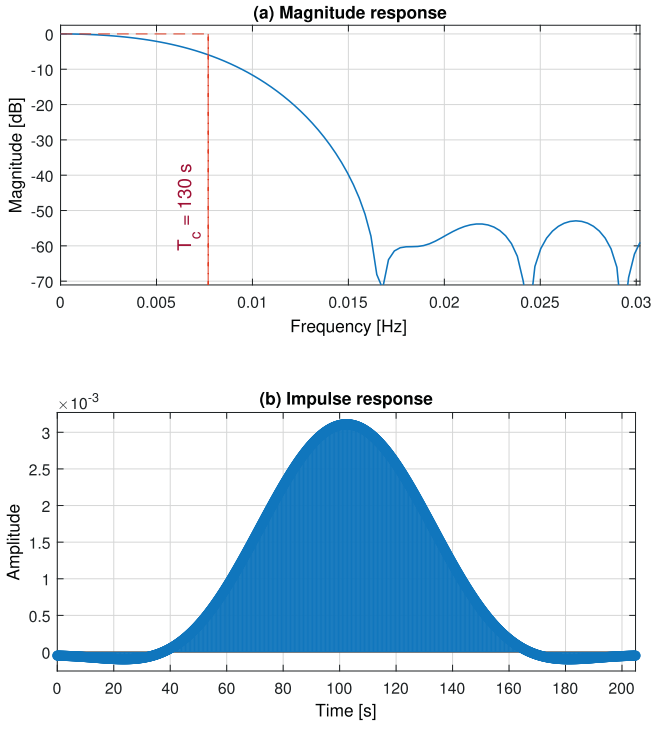

Fig. 3. Low-pass filter applied to the gravity disturbance of the iNAV and the GT-2A: (a) magnitude response with the desired cut-off frequency of 130 s (−6 dB); (b) impulse response.

2.1. Strapdown gravimeter iNAV

The internal sensor assembly (ISA) of the iNAV comprises triads of Honeywell Q-Flex QA-2000 accelerometers and Honeywell GG1320AN ring laser gyroscopes (RLG) (iMAR Navigation, 2012; Johann, 2023), enabling 3-D acceleration and angular rate observations. A geodetic GNSS receiver board for vehicle positioning is integrated within the IMU housing, enabling the tracking of all current GNSS frequencies at a sample frequency of 5 Hz. The IMU is encased in a thermally stabilising housing, the iTempStab-AddOn, which stabilises the ISA temperature to a few tenths of 1 K during typical flight conditions. In collaboration with the Technical University of Dresden, TUDa designed and constructed an uninterruptible power supply (UPS) unit to ensure a continuous power supply from the initial to the final base reading. The assembly (see Fig. 2) is capable of utilising ground, battery, or aircraft power supply and can be installed in a variety of vehicles.

The strapdown observations are processed based on the direct method of strapdown gravimetry where gravity is computed directly in the acceleration domain based on Eq. (1) (Johann, 2023). The direct method was found to perform on par with the indirect method where gravity is obtained in a more complex algorithm indirectly in the position domain through integration of the observed acceleration within a Kalman filter (Johann et al., 2020). GNSS-based position solutions are computed using the Precise Point Positioning (PPP) method with 5 Hz Multi-GNSS observations (GPS, GLONASS, Galileo, BeiDou). The use of freely available precise GNSS orbit and clock products provided by the Center for Orbit Determination in Europe (CODE) enables a kinematic position accuracy of a few centimetres. In the PPP mode, the installation of dedicated base stations in the survey region is not necessary. The position solutions are numerically differentiated to obtain the vehicle velocity and kinematic acceleration. More details on the PPP processing, the numerical differentiation and alternative methods for kinematic acceleration determination can be found in Johann (2023). The navigation-grade specific force and angular rate observations provided by the IMU (iMAR Navigation, 2012) are integrated with the PPP positions to get high-precision attitude estimates of the IMU along the trajectory, without the need for multiple GNSS antennas. PPP processing and GNSS/IMU integration are conducted using the commercial software NovAtel Waypoint Inertial Explorer 8.90.

The processing is completed using MATLAB software developed at TUDa. With the attitude angles, the specific force is rotated to the navigation frame with axis directions North, East, and Down. Gravity disturbance is obtained by subtracting the specific force and normal gravity from the kinematic acceleration. Additionally, the so-called Eötvös correction needs to be applied accounting for the non-inertial, rotating local navigation frame. The linear drift is removed by end-matching the gravity disturbance results to the terrestrial reference gravity at the airfields. Details on the algorithm of the direct method can be found in Johann (2023). The erroneous influence of magnetic fields on the accelerometers of the presented IMU is evaluated and the applied calibration strategy is introduced in Johann et al. (2021). In the survey area of RIISERBATHY, a heading-dependent magnetic field correction of up to ±1.6 mGal is introduced to account for the influence of the Earth's magnetic field.

2.2. Stable platform gravimeter GT-2A

The second gravimeter type used in this study, the GT-2A, was developed and manufactured by NTP Gravimetric Technologies and distributed worldwide by CMG. The gravity sensor is horizontally stabilised and mounted on a rotating table that corrects for rotation around the local vertical axis. This keeps the attitude of the axial-type sensing element with magnetoelectric feedback approximately constant with respect to the local navigation frame (e.g. North/East/Down) (Vitushkin et al., 2022). Compared to its predecessor, the GT-1, the GT-2A features an extended measurement range, which allows measurements in more turbulent flight conditions and flights in draped mode, i.e. following the terrain with a constant vertical separation. Like the strapdown gravimeter, the GT-2A is thermally stabilised.

The drift is ±3 mGal per month (Vitushkin et al., 2022), which is expected to be much lower than for the strapdown gravimeter. Experience has shown that the GT2A's drift may vary considerably along with external ambient temperature, and so the system is operated within a heated external shroud. The GT-2A is heavier than the strapdown gravimeter and more demanding of power, space, and maintenance (see Fig. 2, Table 1). AWI's gravimeter is of the GT-2AP type, which allows high-latitude measurements by GNSS compassing using two or four GNSS antennas (Koneshov et al., 2022). In this survey, however, it was operated with only one antenna for operational reasons and to enable comparability between the GT-2A and iNAV results.

In preparation for the processing of the GT-2A data, the navigational data is processed in differential GNSS (DGNSS) mode using 2 Hz GPS observations with NovAtel Waypoint. The corresponding base station was located at NM-III. The gravity data is processed using software extensions developed by CMG and the University of Moscow, GTNAV/GTGRAV (Krasnov et al., 2022), to integrate closely with the Geosoft Oasis montaj environment. Within this software, a Kalman filter is utilized for adaptive tracking of the aircraft. The gravity data is corrected for latitude, the Eötvös effect, platform tilt, and drift (end-matching).

2.3. Quality analysis

As an indicator of the internal accuracy of the single gravity disturbance results, the precision is obtained by evaluating the residuals at the crossover points of the flight trajectories. Assuming equal precision at both adjacent flight lines, the precision is determined in terms of RMSE, which is the Root Mean Square (RMS) divided by the square root of two. It has been demonstrated by Becker et al. (2015a) that the estimability of the gravity disturbance in strapdown gravimetry is lowered during turns. The estimability indicates if and how well a parameter can be estimated from a given set of observations (Dermanis and Grafarend, 1981). The GT-2A results are dismissed entirely within turns which is a common practice in stable platform gravimetry (Jensen et al., 2019; Petrovic et al., 2015). Therefore, only crossover points at approximately straight lines are included in the crossover evaluation. To limit the impact of discrepancies between the vertical gradient in the normal field and the actual gradient, and the impact of the gravity disturbance attenuation with increasing height depending on the gravitational source wavelength (Childers et al., 1999), crossover points with height differences exceeding 150 m are rejected. The routine removal of crossover points during turns and with large height differences improves the comparability between different airborne campaigns.

Assuming a static gravity field, the gravity disturbance results can be improved by minimising the crossover residuals in a least-squares adjustment (crossover adjustment/levelling). Two methods are applied in this study: Either, one bias is estimated per flight, or one bias is estimated per flight line. In the latter case, a high number of crossover points is required to avoid a distortion of the line network. The application of correction factors that increase the formal crossover point residuals at lines with a small number of crossover points in the RMSE determination according to Becker (2016) avoids overly optimistic RMSE. Note that the adjustment methods are applied in addition to end-matching, i.e. after bias and linear trend removal considering terrestrial reference gravity at the runway. Further details on the crossover adjustment procedure can be found in Johann (2023). The same implementation was used for the crossover evaluation of all solutions in this paper.

Table 1
Characteristics of the gravimeters used in this study (without power supply and control interface; values based on personal experience, Johann, 2023, and Vitushkin et al., 2022).

	iNAV-RQH w. iTempStab-AddOn	GT-2A
Installation	strapdown	stable platform
Measurement principle	3-D quartz accelerometers and 3-D ring laser gyroscopes	1-D sensing element with electromagnetic feedback
Drift	several mGal per day	±3 mGal per month
Dimensions [cm^3]	43 × 25 × 31	40 × 40 × 60 (without rotary table)
Weight [kg]	22	135 (without rotary table)
Power consumption [W]	200 (start-up); 30…90 after stabilisation	150 (plus up to 400 for external heaters)

2.4. Combination approaches

If two or more gravimeters are run simultaneously, the results may be combined to improve the accuracy by taking into account differing wavelength-dependent accuracies of the gravimeters or by reducing the noise in the results through averaging. In this study, three combination approaches were implemented to combine the gravity disturbance results $\delta g_A, \delta g_B$ of two gravimeters A,B. For each gravimeter and flight line, the gravity disturbance results $\delta g_{A,j}, \delta g_{B,j}$ at an epoch j can be split into the arithmetic means μ_A, μ_B of line l and the remainders $r_{A,j}, r_{B,j}$ as

$$\delta g_{A,j} = \mu_{A,l} + r_{A,j}, \text{with } \mu_A = \frac{\sum_{j=1}^{n_l} \delta g_{A,j}}{n_l}$$

$$\delta g_{B,j} = \mu_{B,l} + r_{B,j}, \textit{with } \mu_B = \frac{\sum_{j=1}^{n_l} \delta g_{B,j}}{n_l} \quad (2)$$

with n_l being the number of epochs along the line. The combination approaches are defined as follows (Fig. 4):

(i) "Bias swap": If gravimeter B has a superior long-term stability, the accuracy of gravimeter A can be enhanced by correcting the long-term drift of gravimeter A with data from gravimeter B. A

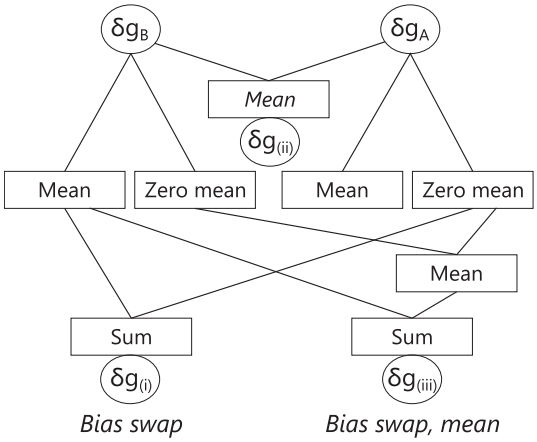

Fig. 4. Combination approaches for two gravity disturbance signals $\delta g_A, \delta g_B$ at a single flight line.

straightforward realisation was successfully implemented by Jensen et al. (2019) where the merged signal

$$\delta g_{(i),j} = \mu_{B,l} + r_{A,j} \tag{3}$$

is primarily based on gravimeter A: The mean value $\mu_{B,l}$ of gravimeter B replaces the mean value of gravimeter A, but the remaining high frequency signal $r_{A,j}$ is taken from gravimeter A.

(ii) "Mean": Here, the gravity disturbance results $\delta g_{A,j}, \delta g_{B,j}$ of both gravimeters are simply averaged as

$$\delta g_{(ii),j} = \frac{\delta g_{A,j} + \delta g_{B,j}}{2} \tag{4}$$

The approach assumes that both gravimeters have similar stochastic properties.

(iii) "Bias swap, mean": This approach combines both (i) and (ii). It assumes that gravimeter B has a more stable long-term drift behaviour, but both gravimeters' short-wavelength results are of similar quality. Accordingly, the mean value $\mu_{B,l}$ of the line is taken from gravimeter B. The short-wavelength results are incorporated by adding the mean of the zero-mean results $r_{A,j}, r_{B,j}$ of both gravimeters as

$$\delta g_{(iii),j} = \mu_{B,l} + \frac{r_{A,j} + r_{B,j}}{2} \tag{5}$$

It is commonly stated that the long-drift behaviour of stable platform gravimeters is superior to those of strapdown gravimeters (e.g. Glennie et al., 2000; Jensen, 2018). Conversely, the latter are assumed to be more resistant to turbulence (e.g. Studinger et al., 2008). In the subsequent analysis, these hypotheses will be assessed for the gravimeters presented in Sections 2.1 and 2.2, employing the introduced combination approaches. The iNAV is designated as gravimeter A, while the GT-2A is designated as gravimeter B.

3. Results

In Section 3.1, the results of the individual gravimeter solutions will be summarised and compared to each other in terms of crossover statistics, their differences, and the influence of flight turbulences. The results will be validated in Section 3.2 through a comparison with the sub-ice topography obtained from radar observations, emphasising the selection of an appropriate low-pass filter length. Section 3.3 will present the results of the combination approaches that were introduced in Section 2.4, with the aim of gaining a deeper understanding of the long- and short-wavelength accuracy of both gravimeters.

The flights will be named according to the day of year. For example, the flight conducted on 31 December 2022 will be designated "365", while the flight on 5 January 2023 will be designated "5". The term "(flight) line" will be used to describe approximately straight trajectory segments.

As indicated in Sections 2.1 and 2.2, different GNSS receivers and two distinct GNSS positioning methods, PPP with Multi-GNSS 5 Hz sampling and DGNSS with GPS-only 2 Hz sampling, were used for the iNAV and the GT-2A, respectively. To assess the influence of the GNSS solutions on the gravity disturbance results, the iNAV gravity processing was also executed using the GT-2A DGNSS solutions as a trial. The RMSE of the iNAV gravity disturbance difference between the PPP 5 Hz Multi-GNSS and the DGNSS 2 Hz GPS-only solutions was about 0.37 mGal. Hence, the influence of the GNSS processing on the overall precision is assumed insignificant in the evaluated campaign. The main precision differences are expected to depend on the gravimeter types and the gravity processing. However, in other campaigns with different gravimeters and flight conditions, the influence of the GNSS processing method can be higher (Johann, 2023; Li et al., 2018; Zhang et al., 2017). No major GNSS issues due to the low satellite elevation in Antarctica occurred.

3.1. Individual results and comparison

The gravity disturbance obtained with the iNAV strapdown gravimeter (Johann et al., 2025) is illustrated in Fig. 5a. The results span a range of more than 250 mGal. With approximately 180 crossover points, the RMSE of these points is expected to serve as a robust precision indicator. In the end-matching procedure of the ten flights, linear drifts between −13.0 and +6.7 mGal per day were removed between the alignment periods at the airfield (mean of absolute drifts: 4,1 mGal/d).

Without crossover adjustment, the RMSE for the iNAV is 1.71 mGal. It improves significantly to 1.07 mGal when a bias per flight is estimated (flight-wise adjustment). Estimating a bias per line (line-wise adjustment) gives only a minor improvement to 1.01 mGal. As the number of crossovers is high and there is only one intra-flight crossover, almost all crossovers and lines can be used in the adjustments. Note that in this evaluation, all residuals at the flight lines with a maximum height difference of 150 m are included; no outliers are removed. However, it should be mentioned that the precision improves significantly when flight 1 is removed. With about 145 crossovers remaining, the RMSE before adjustment becomes 1.37 mGal, and 0.96 mGal (0.88 mGal) after flight-wise (line-wise) adjustment.

With 2.40 mGal, the internal crossover RMSE of the GT-2A results (Eisermann et al., 2025a) is slightly worse than that of the iNAV (Table 2, blue and red bars in Fig. 6). While a flight-wise adjustment does not result in enhancement of the GT-2A precision, a line-wise adjustment improves the RMSE to 1.99 mGal. The RMSE of the adjusted results of the iNAV is thus considerably better than that of the GT-2A. Flight 1 is less conspicuous than for the iNAV.

In addition to the internal crossover RMSE, the difference between the iNAV and the GT-2A gravity disturbance solutions along the trajectory is evaluated (Fig. 5b). Fig. 7 depicts the mean values and standard deviations of the difference for all flights. The total mean is 1.96 mGal and the standard deviation is 3.04 mGal. Due to the high mean value, the RMS of the difference (3.62 mGal) is higher than the internal crossover RMS of the iNAV (2.42 mGal) and the GT-2A (3.39 mGal). Note that the RMS, rather than the RMSE, is calculated here since equal precision cannot be presumed for both gravimeters. Without flight 1, the agreement between the individual internal RMS (1.94 mGal for the iNAV, 3.31 mGal for the GT-2A) and the RMS of the differences (3.07 mGal) improves considerably.

Fig. 8a visualises the amplitude spectrum of the iNAV gravity disturbance results that were obtained at the south-eastern flight line (black polygons in Fig. 5) after 100 s low-pass filtering. The figure reveals that the bulk of the signal content is found at frequencies lower than 2 mHz which corresponds to a wavelength longer than 500 s and, considering the flight velocity, a spatial resolution (half wavelength) of more than 19 km. The corresponding amplitude spectrum of the GT-2A is not shown, because the differences to the iNAV would not be visually recognisable. Instead, the difference between the spectra is shown in Fig. 8b, with an adapted scaling. While there does not exist an obvious frequency-dependent systematic difference between the gravimeters, the differences tend to slightly increase with increasing frequencies until the frequencies approach the cut-off frequency (100 s) of the evaluated low-pass filtered gravity disturbance results.

The RMS-g is the moving standard deviation of the GNSS-derived vertical kinematic acceleration and can be used as an indicator of turbulence (Becker, 2016). It should be noted that high GNSS noise may also contribute to an increased RMS-g. In the scope of the RIISERBATHY campaign and in Johann (2023), a moving window length of 50 s was selected for RMS-g computation. Only 1 Hz kinematic acceleration was used as input to maximise comparability with previous campaigns. With (240 ± 131) mm/s^2 (mean and one sigma standard deviation), the average RMS-g along all flights of the RIISERBATHY campaign was

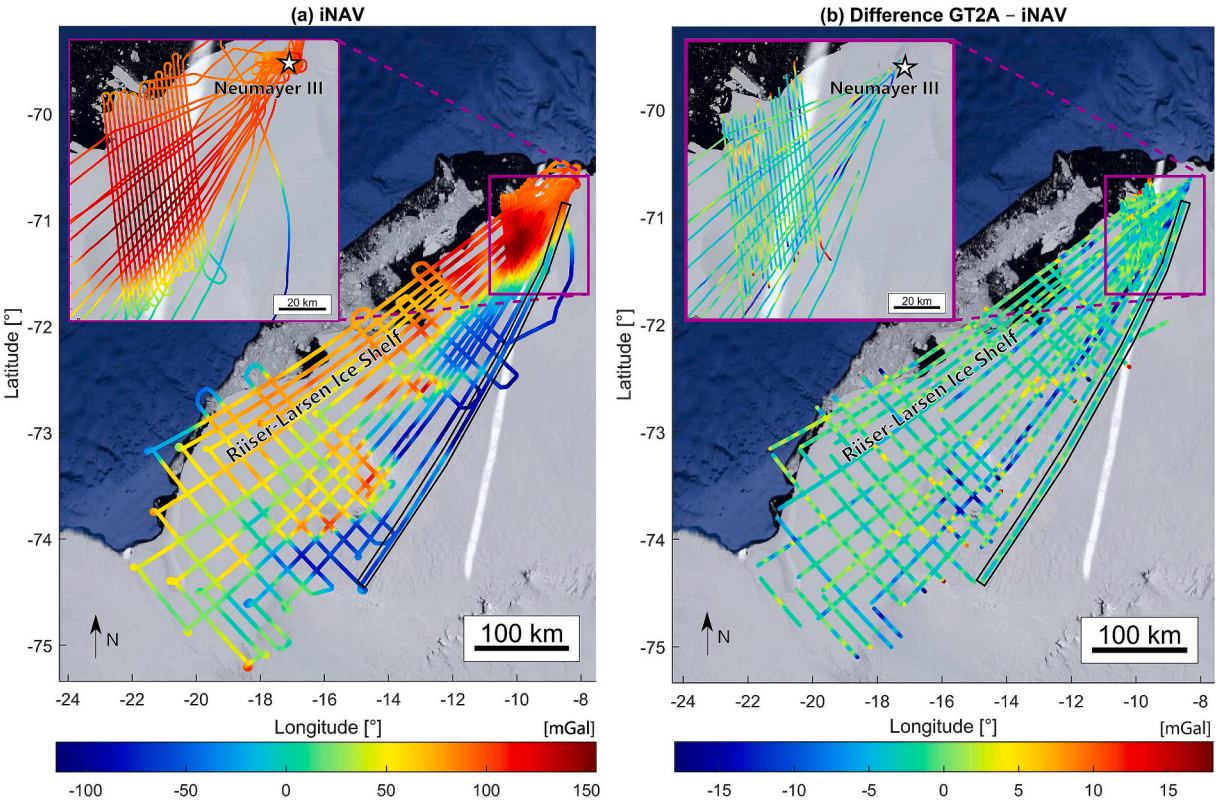

Fig. 5. Non-adjusted gravity disturbance results (down) (purple rectangle: enlarged map extract of the dense grid at the airfield in the vicinity of the Neumayer-III station; line surrounded by black polygon compared with topography in Section 3.2 and used in Figs. 8 and 10): (a) iNAV only; (b) difference between GT-2A and iNAV (map data: Google, U.S. Geological Survey). (For interpretation of the references to colour in this figure legend, the reader is referred to the web version of this article.)

Table 2
RMSE of individual and combined solutions based on the crossover point residuals of all flights (all values in mGal).

Adjustment	iNAV	GT-2A	Combination (i) (bias swap)	Combination (i) reverse order	Combination (ii) (mean)	Combination (iii) (bias swap, mean)	Combination (iii) reverse order
None	1.71	2.40	1.42	2.44	1.39	1.53	1.70
Flight-wise	1.07	2.41	1.33	2.10	1.22	1.49	1.10
Line-wise	1.01	1.99	1.02	1.99	1.02	1.02	1.02

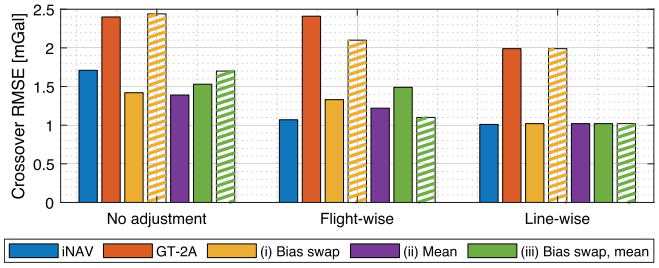

Fig. 6. Crossover point RMSE for individual gravimeter solutions and combination approaches (i), (ii), and (iii) (hatched: reverse gravimeter order, i.e. line bias taken from iNAV instead of GT-2A)

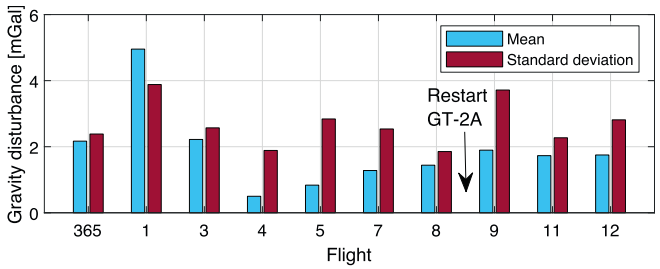

Fig. 7. Mean and standard deviation of the difference between the iNAV and GT-2A non-adjusted gravity disturbance results (iNAV – GT-2A), separated by flights (the GT-2A was restarted after flight 8).

among the lowest values of recent campaigns with the iNAV (Johann, 2023) indicating a generally low turbulence level. However, a comparison of possible dependencies between the RMS-g and the obtained gravity disturbance precision is of interest. Fig. 9 visualises the absolute crossover residuals as a function of the mean RMS-g values of both adjacent lines at the intersection epochs. The mean residuals in 50 mm/s^2 intervals are indicated by bold rings. Both gravimeters tend to show a similar increase in the residuals with increasing RMS-g. Therefore, for the depicted low and medium RMS-g levels, both gravimeters respond similarly to increased turbulence. However, in all intervals, the mean residuals of the GT-2A are slightly larger than those of the iNAV. Hence, the overall error in the gravity disturbance results is higher for the GT-2A. Note that RMS-g values beyond 100 and 350 mm/s^2 are not included in Fig. 9 due to the small number of samples here. The response to higher RMS-g may hence differ between the two gravimeters.

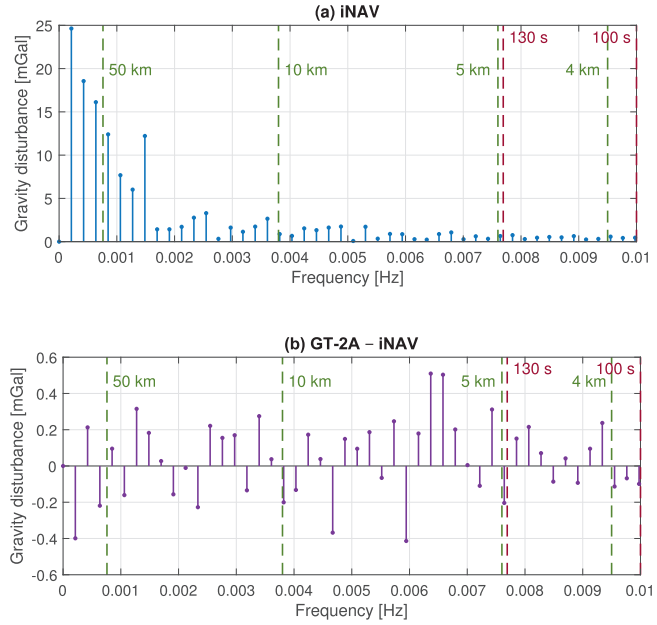

Fig. 8. Amplitude spectra of the 100 s filtered gravity disturbance of the south-eastern flight line with filter wavelengths (red) and spatial resolutions (half wavelength, green) corresponding to the signal frequency: (a) iNAV; (b) difference between GT-2A and iNAV (new scaling). (For interpretation of the references to colour in this figure legend, the reader is referred to the web version of this article.)

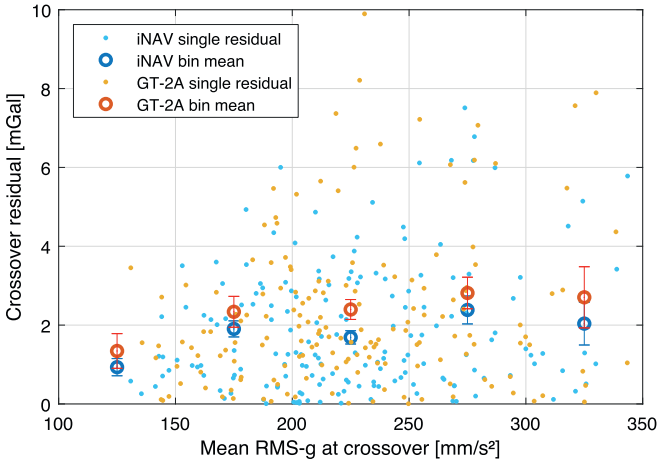

Fig. 9. Absolute non-adjusted crossover point residuals as a function of the mean turbulence of both adjacent flight lines (rings: mean values and their one sigma standard deviations of all residuals in 50 mm/s^2 bins).

3.2. Comparison with topography

Variations in the true gravity disturbance signal are primarily attributed to the influence of varying topography and heterogenous subsurface density. A comparison of the observed gravity disturbance with topography may indicate whether observed variations in the gravity disturbance results can be explained by topography or whether they are due to other effects, such as sensor noise, density variations or lateral gravitation. Consequently, the evaluation may also prove beneficial in the selection of appropriate low-pass filter lengths.

In the RIISERBATHY campaign, the low-pass filter length was set to 130 s. The application of shorter and longer filter lengths resulted in a degradation in terms of crossover RMSE, indicating that a filter length of 130 s represents an optimal compromise between the suppression of noise and the preservation of true short-wavelength signals. The GT-2A results were subjected to the same filter (see Section 2, Fig. 3). To investigate whether small topographic features can be better identified with a shorter filter length, both gravimeters were alternatively filtered with 100 s low-pass filters. At an average speed of 76 m/s, the nominal spatial resolutions for the results filtered with the 130 s and 100 s filters are 4.9 km and 3.8 km, respectively. When using 100 s instead of 130 s filters, the crossover RMSE degraded from 1.71 to 1.83 mGal for the iNAV, and from 2.40 to 2.72 mGal for the GT-2A. It should be noted that the optimal filter length may vary in other campaigns, depending on the gravity field variability, the flight conditions, and the flight velocity.

For the comparison, the longest flight line above grounded ice was selected (black polygons in Fig. 5). It was flown from North-East to South-West. The gravity disturbance results of both gravimeters with both filter lengths are illustrated in Fig. 10a, along with the global model XGM2019e (Zingerle et al., 2020; Zingerle et al., 2019), which was obtained through the International Centre for Global Earth Models (ICGEM) (Ince et al., 2019). XGM2019e is modelled as a spheroidal harmonic expansion up to degree and order 5399, which corresponds to a nominal spatial resolution of about 4 km. However, in the campaign region, XGM2019e is based on satellite gravimetry (GOCE and GRACE) and a 15′ gravity grid, corresponding to a lower spatial resolution of about 28 km, obtained from airborne gravimetry surveys with accuracies of 4 and 10 mGal in the survey area (Scheinert et al., 2016). Fig. 10b shows the corresponding ice surface, derived from the photogrammetry-based digital elevation model REMA with a spatial resolution of 2 m (Howat et al., 2022a, 2022b; Howat et al., 2019), and the sub-ice topography obtained from RIISERBATHY radar measurements using AWI's EMR radar system (Nixdorf et al., 1999; Steinhage, 2001; Eisermann et al., 2025b), which was employed in toggle mode. The anticipated vertical accuracy of the EMR-derived depths is about 20 m. Line sections with gaps in the radar data are greyed in Fig. 10.

The variability of the ice base is much greater than that of the ice surface (see Fig. 10b). Therefore, the correlation between the observed gravity disturbance and the topography is more pronounced than that observed with the ice surface (see Fig. 10a). There is a high degree of agreement between the iNAV and GT-2A data along the trajectory. Both gravimeters display greater detail in the short-wavelength information than the global model XGM2019e. The large downward trend in the gravity disturbance until line km 200 (see Fig. 10a) does not agree with the local topography (see Fig. 10b). It is assumed to be due to a basaltic wedge in the Weddell Sea parallel to the calving line which causes the Explora anomaly (Jokat et al., 2004). The flight line starts at the Explora anomaly where the gravity disturbance is expected to be higher due to the high density of the igneous rocks. Along the flight line, the distance to the Explora anomaly increases resulting in a decrease in gravity disturbance.

As expected, a short low-pass filter length of 100 s (dashed line) results in more short-wavelength variations. Except for line km 360 and greater, the higher variations do not align better with the topographic variations in most segments. Although the remaining short-wavelength variations may originate from sub-surface density variations or topographic variations lying out of the plane of the displayed profile, the unchanged agreement with the shown topography and the worse crossover RMSE at the 100 s filter length indicate that most of these variations are due to sensor noise superimposing the true short-wavelength gravity signal. This corroborates the selection of the 130 s filter length, yielding a spatial resolution of 4.9 km.

3.3. Combination

The individual and combined gravity disturbance results of the five approximately straight flight lines of flight 12 are shown in Fig. 11a. This flight is selected as an example because the mean and standard deviation of the difference between the iNAV and GT-2A results are close to those of the total campaign (see Fig. 7). In most trajectory segments,

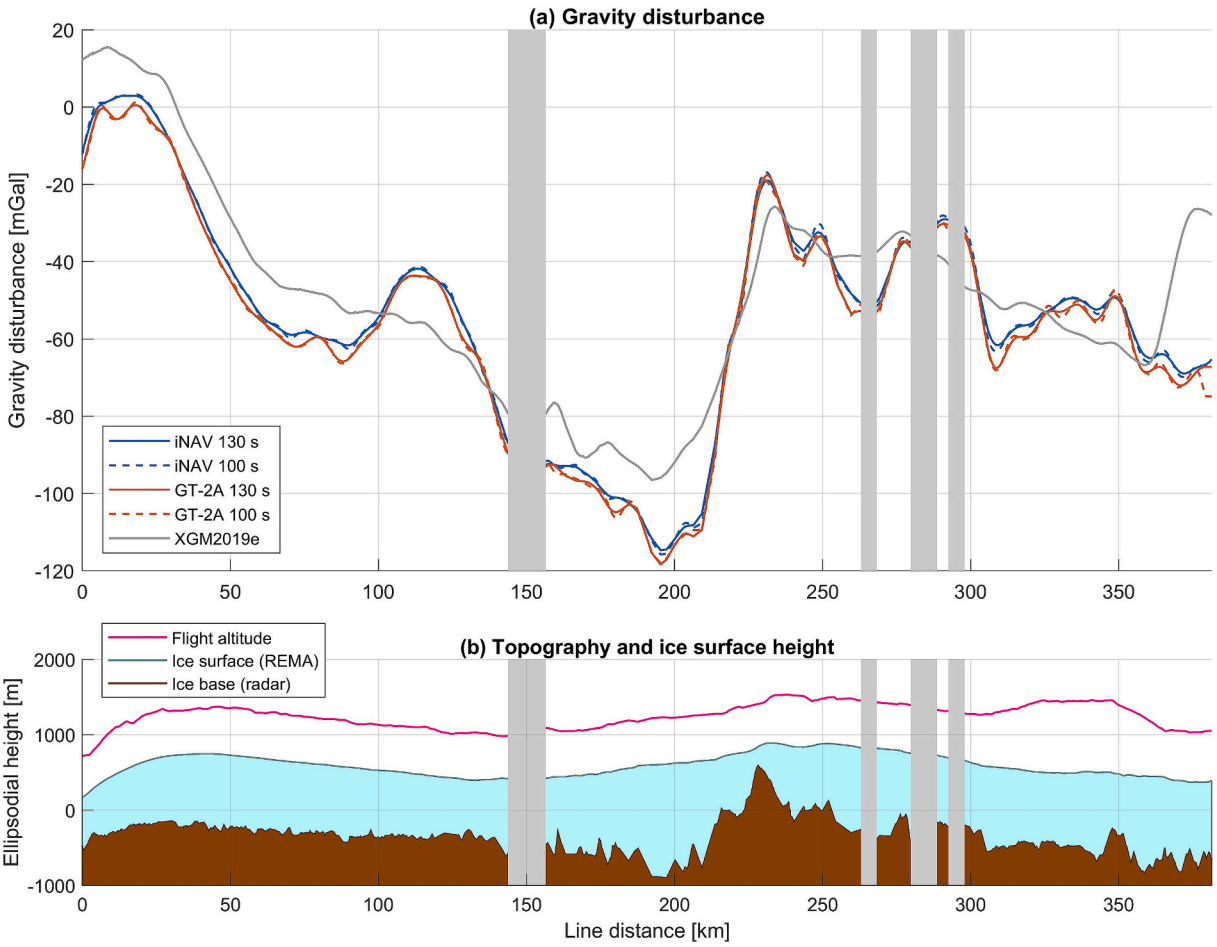

Fig. 10. Non-adjusted gravity disturbance results of the south-eastern flight line with corresponding topography beneath the grounded ice, ice surface height, and aircraft altitude.

the results agree well. Again, the spatial resolution and accuracy is understood to be much better than for the global model XGM2019e.

The differences between the results are visualised in Fig. 11b, wherein the mean of the two individual gravimeter solutions, i.e. the combination approach (ii), is employed as reference. The blue and red lines illustrate the discrepancy between the individual gravimeter solutions and their mean. Biases between both gravimeters are evident for the first three lines, whereas they are negligible in lines 4 and 5. The differences between the combination approaches are also shown in Fig. 11b. The results of combination approach (i) (bias swap, yellow line), where the bias is taken from the GT-2A and the high frequency results are taken from the iNAV, meet the expectations: the line mean values are equal to the GT-2A results and deviations are equal to those of the shifted iNAV results. Combination approach (ii) (purple line) simply takes the mean of both individual results. As it is taken as reference here, it is zero at all lines in Fig. 11b. Combination approach (iii) (green line) combines the other approaches. It forms the mean of the high frequency parts of both gravimeters at each line, resulting in a constant shift when compared to approach (ii) (purple). Also, the line mean values are equal to those of the GT-2A (red) and combination approach (i) (yellow) since the bias is taken from the GT-2A.

The properties and quality of the single and combined solutions are further investigated by analysing the crossover residual distributions of the individual flight lines (Fig. 12) and the crossover RMSE of each solution (see Fig. 6, Table 2). Fig. 12a-b indicates that flight-dependent biases are higher for the iNAV than for the GT-2A, but the general noise is lower for the strapdown device. This agrees with the findings presented in Section 3.1. Without crossover adjustment, the crossover RMSE of the individual solutions (1.71 mGal for the iNAV, 2.40 mGal for the GT-2A) are significantly improved after combination to 1.42, 1.39 mGal and 1.70 mGal for the approaches (i), (ii), and (iii), respectively (see Fig. 6, Table 2, and Fig. 12c-e). The combinations with the designated gravimeter orders (filled bars in Fig. 6) are approximately on a par, with the simple mean approach (ii) exhibiting a slight advantage. If the gravimeter order in the approaches (i) and (iii) is reversed (hatched bars in Fig. 6), i.e. the line biases are taken from the iNAV, then the RMSE are worse than those in the designated order.

The long-term drift behaviour is analysed in more detail by evaluating the flight-wise and line-wise adjusted crossover RMSE of each solution. After flight-wise adjustment, the differences between the combination methods increase slightly. Approach (i) (1.33 mGal), using full high frequency data from the iNAV, performs better than approach (iii) (1.49 mGal). The best combined results are obtained using the simple mean combination (ii) (1.22 mGal) suggesting that the assumptions about the long- and short-term stabilities of the two gravimeters are not entirely correct. If the order in approach (i) is reversed, i.e. the full high frequency data is taken from the GT-2A (hatched yellow bar in Fig. 6), the worst combination result (2.10 mGal) is obtained due to the high noise level of the GT-2A. However, if the order is reversed for approach (iii), i.e. the line means are taken from the iNAV after removing a flight-wise bias and the averaged high frequency data from both gravimeters are added, the best result is obtained (1.10 mGal).

After line-wise adjustment, where a bias is estimated for each line, the crossover RMSE depends entirely on the high frequency part of the selected data. Consequently, equal RMSE of 1.02 mGal are obtained for the individual iNAV solution and the combination approach (i). The GT-

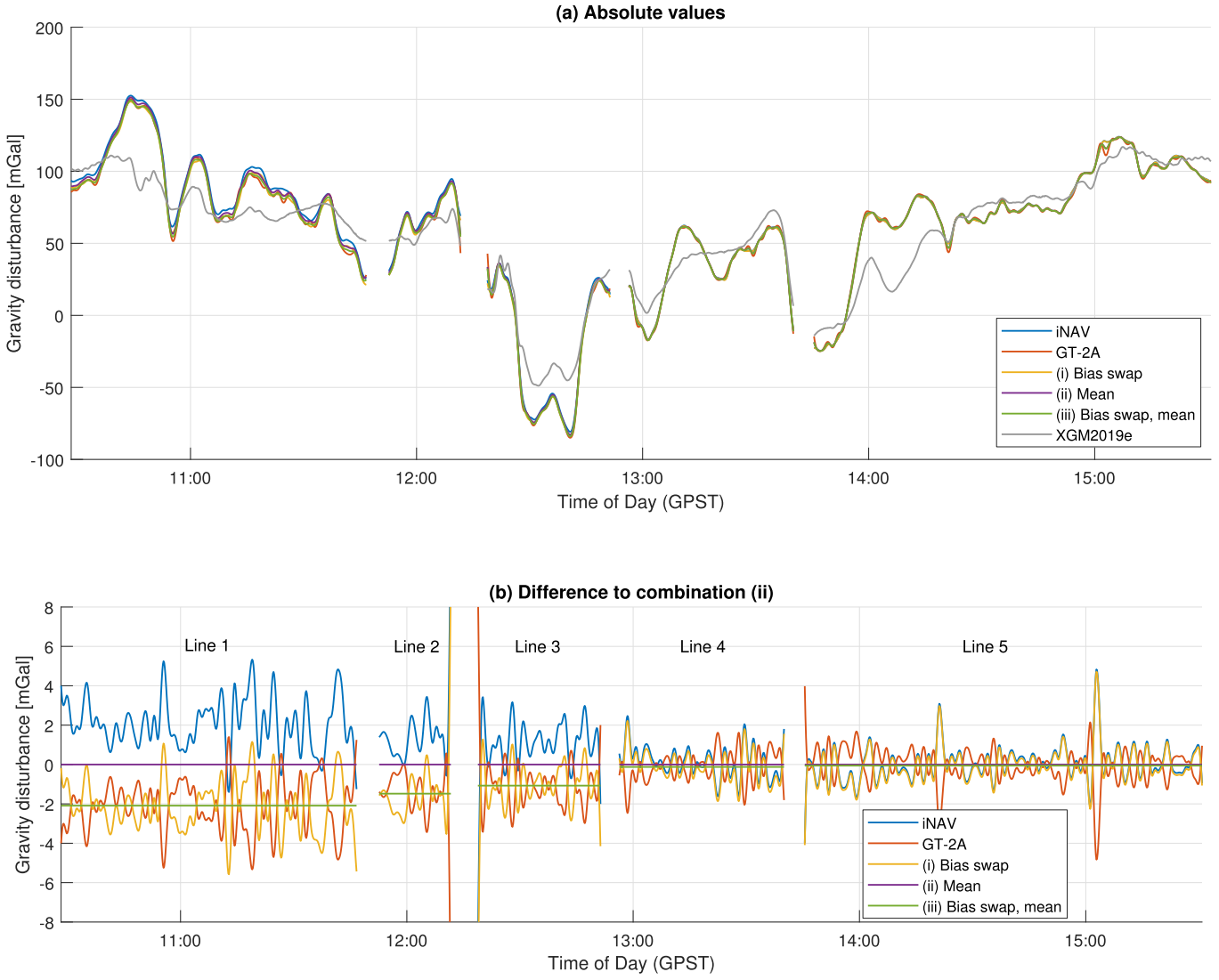

Fig. 11. Non-adjusted gravity disturbance results at the flight lines of flight 12: (a) absolute values and (b) differences to combination approach (ii), i.e. the mean of both gravimeters' individual results.

2A based solutions, i.e. the individual solution and the reverse approach (i), have RMSE of 1.99 mGal. Although the differences between the two line-wise adjusted gravimeter solutions are large, the solutions with averaged high frequency noise, i.e. approaches (ii) and (iii), are on par with the iNAV-only solution (1.0 mGal).

4. Discussion

The evaluation of the non-adjusted and adjusted crossover point residuals for the combination approaches leads to the following key findings:

- For the heterogeneous, non-adjusted iNAV and GT-2A data, all the combination approaches introduced yield significant improvements in precision. Especially in campaigns with many lines with a small number of crossover points, where a crossover adjustment is not possible, similar combinations of two gravimeters might be advisable.
- Without adjustment, the simple mean approach results in the best precision. This suggests that the hypothesis that the long-wavelength drift behaviour of the GT-2A was superior within the flights may not be true. However, the comparatively bad precision for the results where the biases are taken from the iNAV (hatched bars in Fig. 6) indicate deficiencies in the long-term stability of the iNAV.
- While the RMSE of the GT-2A remains approximately unchanged after flight-wise adjustment, the RMSE of the iNAV improves significantly. Conversely, after line-wise adjustment, the RMSE of the GT-2A improves more. The results after flight-wise adjustment show the best results when the line means are taken from the iNAV, and the remaining high frequency data are averaged from both gravimeters. These observations indicate that, in the RIISERBATHY campaign, the iNAV results are affected by significant flight-to-flight biases, even after end-matching, but that its medium and short wavelength results are superior to the results of the GT-2A. Even the line-to-line stability of the strapdown device outperforms that of the stable platform gravimeter here.
- Although the high frequency noise levels of the two gravimeters are very different, the combination leads to slight improvements in the line-wise adjusted result. A gravimeter combination might be even more advantageous if two gravimeters with similar low noise levels were combined.

For the iNAV, flight 1 exhibited worse precision than the other flights. This might be due to a higher turbulence level in terms of RMS-g

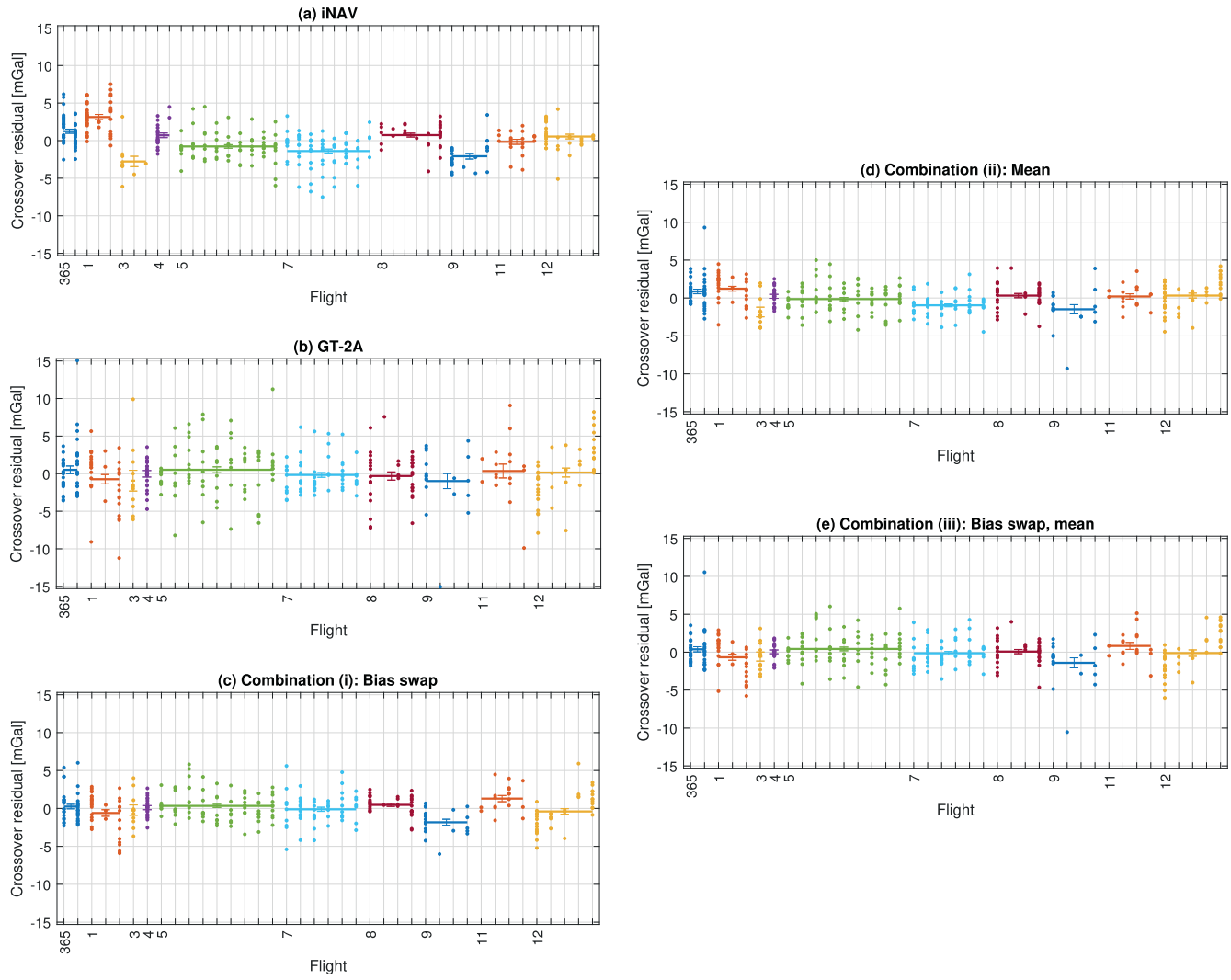

Fig. 12. Non-adjusted crossover residuals sorted by flights (indicated by the colour) and lines (one column per line; horizontal bars: mean values of the flights with their one sigma standard deviations; each crossover residual is displayed at both adjacent lines, with opposite sign).

in the second half of flight 1 or an unknown extraordinary systematic effect. The high standard deviation of the difference at flight 9 (see Fig. 7) is suspected to be caused by a restart of the GT-2A after flight 8, as evidenced by the observation that a removal of this flight leads to stronger internal precision improvements for the GT-2A than for the iNAV.

5. Conclusions and outlook

The GT-2A stable platform gravimeter and the iMAR iNAV-RQH-1003 strapdown gravimeter equipped with iTempStab-AddOn, were tested in an airborne campaign over East Antarctica. Under polar conditions, without crossover adjustment, crossover RMSE of 1.71 and 2.40 mGal resulted for the iNAV and the GT-2A, respectively. Both gravimeters exhibited comparable responses to the observed low and medium turbulence conditions. A crossover evaluation and comparison with topography of grounded ice revealed that a filter length of 130 s is a suitable compromise between noise reduction and preservation of the short-wavelength gravity signal. In other campaigns, the optimal filter length may vary depending on the specific flight conditions and gravity field characteristics.

An analysis of flight- and line-wise crossover adjustment revealed that, on the one hand, the iNAV results exhibit superior short-term stability and smaller line-to-line biases compared to the GT-2A. On the other hand, systematic flight biases appear in the iNAV results, which can be mitigated by estimating a single bias per flight (flight-wise adjustment) but should be further investigated. Notwithstanding these limitations, the high overall precision, and advantages in terms of weight, size, and operation have seen strapdown sensors advance towards being the preferred choice for gravimetry in recent years.

Several approaches for combining the results of both gravimeters were introduced and implemented. Despite the significant differences in noise levels between the two gravimeters, all approaches resulted in improved outcomes compared to the single-gravimeter results without adjustment. After adjustment, a crossover precision of about 1.0 mGal was achieved. If the frequency-dependent noise behaviours of two gravimeters differ significantly, a careful selection of the low- and high-wavelength result parts of both gravimeters yields the best results. Otherwise, a simple mean can be sufficient. Combining two or more high-precision gravimeters or devices with multiple vertical accelerometers may be even more effective for sensors with similar accuracy.

Declaration of generative AI and AI-assisted technologies in the writing process

During the preparation of this work the authors used DeepL Write and Chat AI (KISSKI/GWDG) in order to improve the readability and language of the manuscript written by the authors. After using these

tools, the authors reviewed and edited the content as needed and take full responsibility for the content of the published article.

Funding

The airborne campaign RIISERBATHY was jointly funded by the Alfred Wegener Institute (AWI) and the German Federal Institute for Geosciences and Natural Resources (BGR). HE is funded through the INSPIRES program at the Alfred Wegener Institute.

CRediT authorship contribution statement

Felix Johann: Conceptualization, Methodology, Validation, Formal analysis, Writing – original draft, Visualization. **Hannes Eisermann:** Conceptualization, Investigation, Writing – review & editing. **Graeme Eagles:** Conceptualization, Investigation, Writing – review & editing.

Declaration of competing interest

The authors declare that they have no known competing financial interests or personal relationships that could have appeared to influence the work reported in this paper.

Acknowledgements

The authors would like to express their gratitude to the pilots and crew of Kenn Borek, Air Ltd., Canada, the logistical and technical personnel at AWI, Neumayer-III, and Troll station for their invaluable support during the RIISERBATHY campaign. Particularly, the authors gratefully acknowledge Christoph Petersen and Dennis Ludwig from the AWI for their technical assistance in the preparation for the campaign and during the fieldwork. Moreover, the authors would like to express their gratitude to Helen Tuckett and Wayne Hewison of Transparent Earth Geophysics, Australia, for their valuable support in the GT-2A processing. The authors would also like to thank the associate editor and the reviewers for their profound and in-depth comments, which contributed to various enhancements of the manuscript.

Data availability

The newly acquired gravity data of the iNAV (Johann et al., 2025) and GT-2A (Eisermann et al., 2025a) gravimeters, and ice thickness data (Eisermann et al., 2025b) are deposited at PANGAEA. The used auxiliary topographic data set is REMA DEM V2 (Howat et al., 2022b).

References

Becker, D., 2016. Advanced Calibration Methods for Strapdown Airborne Gravimetry. Technische Universität Darmstadt, Darmstadt.

Becker, D., Becker, M., Leinen, S., Zhao, Y., 2015a. Estimability in strapdown airborne vector gravimetry. In: International Association of Geodesy Symposia. https://doi.org/10.1007/1345_2015_209.

Becker, D., Nielsen, J.E., Ayres-Sampaio, D., Forsberg, R., Becker, M., Bastos, L., 2015b. Drift reduction in strapdown airborne gravimetry using a simple thermal correction. J. Geod. 89, 1133–1144. https://doi.org/10.1007/s00190-015-0839-8.

Cao, J., Meng, Y., Cui, X., Zhao, X., Cai, S., Yu, R., Pang, X., 2023. A Flight Test of Airborne Gravimetry in Antarctic, 12551, p. 44. https://doi.org/10.1117/12.2668154.

Childers, V.A., Bell, R.E., Brozena, J.M., 1999. Airborne gravimetry: an investigation of filtering. Geophysics 64. https://doi.org/10.1190/1.1444530.

Dermanis, A., Grafarend, E.W., 1981. Estimability analysis of geodetic, astrometric and geodynamical quantities in very long baseline interferometry. Geophys. J. Int. 64 (1), 31–56. https://doi.org/10.1111/j.1365-246X.1981.tb02657.x.

Dierssen, H.M., Theberge, A.E., 2014. Bathymetry: assessment. Encycl. Nat. Resour. Water. https://doi.org/10.1081/E-ENRW-120048588.

Eisermann, H., 2021. Topography beneath the Ice Shelves and Ice Sheets of Dronning Maud Land : Implications for Ice Shelf Stability and Glacial History. https://doi.org/10.26092/elib/1481.

Eisermann, H., Eagles, G., Ruppel, A., Smith, E.C., Jokat, W., 2020. Bathymetry beneath ice shelves of Western Dronning Maud Land, East Antarctica, and implications on ice shelf stability. Geophys. Res. Lett. 47. https://doi.org/10.1029/2019GL086724.

Eisermann, H., Eagles, G., Jokat, W., 2024. Coastal bathymetry in central Dronning Maud Land controls ice shelf stability. Sci. Rep. 14, 1–13. https://doi.org/10.1038/s41598-024-51882-2.

Eisermann, H., Ruppel, A., Eagles, Graeme, Läufer, A., 2025a. Airborne Gravity Data (GT-2A) Across Riiser-Larsen Ice Shelf, East Antarctica, from 2022/23 (RIISERBATHY Project) [Data set]. PANGAEA (datast in review). https://doi.pangaea.de/10.1594/PANGAEA.971553.

Eisermann, H., Ruppel, A., Eagles, G., Läufer, A., Steinhage, D., Helm, V., Franke, S., 2025b. ANT 2022/23: AWI airborne Radio-Echo Sounding data across Riiser-Larsen Ice Shelf, East Antarctica, from 2022/23 (RIISERBATHY Project) [Data set]. PANGAEA (datast in review). https://doi.pangaea.de/10.1594/PANGAEA.971622.

Forsberg, R., Olesen, A.V., 2010. Airborne gravity field determination. In: Xu, G. (Ed.), Sciences of Geodesy - I: Advances and Future Directions. Springer, Berlin, pp. 83–104. https://doi.org/10.1007/978-3-642-11741-1_3.

Förste, C., Ince, E.S., Johann, F., Schwabe, J., Liebsch, G., 2020. Marine gravimetry activities on the Baltic Sea in the framework of the EU project FAMOS. Zeitschrift für Geodäsie, Geoinformation und Landmanagement 145, 287–294. https://doi.org/10.12902/zfv-0317-2020.

Glennie, C.L., Schwarz, K.P., Bruton, A.M., Forsberg, R., Olesen, A.V., Keller, K., 2000. A comparison of stable platform and strapdown airborne gravity. J. Geod. 74, 383–389. https://doi.org/10.1007/s001900000082.

Howat, I.M., Porter, C., Smith, B.E., Noh, M.J., Morin, P., 2019. The reference elevation model of Antarctica. Cryosphere 13, 665–674. https://doi.org/10.5194/tc-13-665-2019.

Howat, I.M., Porter, C., Noh, M.J., Husby, E., Khuvis, S., Danish, E., Tomko, K., Gardiner, J., Negrete, A., Yadav, B., Klassen, J., Kelleher, C., Cloutier, M., Bakker, J., Enos, J., Arnold, G., Bauer, G., Morin, P., 2022a. The Reference Elevation Model of Antarctica - Mosaics, Version 2. https://doi.org/10.7910/DVN/EBW8UC.

Howat, I.M., Porter, C., Noh, M.J., Husby, E., Khuvis, S., Danish, E., Tomko, K., Gardiner, J., Negrete, A., Yadav, B., Klassen, J., Kelleher, C., Cloutier, M., Bakker, J., Enos, J., Arnold, G., Bauer, G., Morin, P., 2022b. The Reference Elevation Model of Antarctica - Mosaics, Version 2 [Data Set]. Harvard Dataverse. https://doi.org/10.7910/DVN/EBW8UC.

IMAR Navigation, 2012. iNAV-RQH-1003: Inertial Measurement System for Advanced Applications [WWW Document]. https://www.imar-navigation.de/downloads/NAV_RQH_1003_en.pdf (accessed 5.17.24).

Ince, E.S., Barthelmes, F., Reißland, S., Elger, K., Förste, C., Flechtner, F., Schuh, H., 2019. ICGEM – 15 years of successful collection and distribution of global gravitational models, associated services, and future plans. Earth Syst. Sci. Data 11, 647–674. https://doi.org/10.5194/essd-11-647-2019.

Jensen, T.E., 2018. Airborne Strapdown Gravity Measurements for Geodesy and Geophysics. Technical University of Denmark.

Jensen, T.E., Nielsen, J.E., Olesen, A.V., Forsberg, R., 2017. Strapdown airborne gravimetry using a combination of commercial software and stable-platform gravity estimates. In: International Association of Geodesy Symposia. https://doi.org/10.1007/1345_2017_9.

Jensen, T.E., Olesen, A.V., Forsberg, R., Olsson, P.A., Josefsson, Ö., 2019. New results from strapdown airborne gravimetry using temperature stabilisation. Remote Sens. 11, 1–19. https://doi.org/10.3390/rs11222682.

Johann, F., 2023. Magnetic Calibration and GNSS Processing in Strapdown Dynamic Gravimetry. Technical University of Darmstadt. https://doi.org/10.26083/tuprints-00024342.

Johann, F., Becker, D., Becker, M., Ince, E.S., 2020. Multi-scenario evaluation of the direct method in strapdown airborne and shipborne gravimetry. In: International Association of Geodesy Symposia. Springer, Berlin, Heidelberg, pp. 1–8. https://doi.org/10.1007/1345_2020_127.

Johann, F., Becker, D., Becker, M., Hoss, M., Löwer, A., Förste, C., 2021. The influence of the Earth's magnetic field on strapdown inertial gravimetry using Q-Flex accelerometers: static and dynamic experiments. J. Geod. 95, 1–15. https://doi.org/10.1007/s00190-021-01553-1.

Johann, F., Eisermann, H., Eagles, G., 2025. Airborne strapdown gravity disturbance data (iNAV) across Riiser-Larsen Ice Shelf, East Antarctica, from 2022/23 (RIISERBATHY Project) [Data set]. PANGAEA. https://doi.org/10.1594/PANGAEA.974371.

Jokat, W., Ritzmann, O., Reichert, C., Hinz, K., 2004. Deep crustal structure of the continental margin off the Explora Escarpment and in the Lazarev Sea, East Antarctica. Mar. Geophys. Res. 25, 283–304. https://doi.org/10.1007/s11001-005-1337-9.

Kazama, T., Aoyama, Y., Fukuda, Y., Doi, K., 2019. Absolute gravity and GNSS measurements on bedrock outcrops in Dronning Maud Land, East Antarctica. In: Japan Geoscience Union Meeting 2019. Japan Geoscience Union.

Koneshov, V.N., Pogorelov, V.V., Solovev, V.N., Krasnov, A.A., Sokolov, A.V., Golovan, A.A., Smoller, Y., Yurist, S., 2022. Studying the gravity field in hard-to-reach areas of the earth. In: Peshekhonov, V.G., Stepanov, O.A. (Eds.), Methods and Technologies for Measuring the Earth's Gravity Field Parameters2. Springer Nature, Cham, pp. 199–236. https://doi.org/10.1007/978-3-031-11158-7_4.

Krasnov, A., Sokolov, A., Bolotin, Y., Golovan, A., Parusnikov, N., Motorin, A., Nosov, A., Stepanov, O.A., Yurist, S., Vyazmin, V., 2022. Data processing methods for onboard gravity anomaly measurements. In: Peshekhonov, V.G., Stepanov, O.A. (Eds.), Methods and Technologies for Measuring the Earth's Gravity Field Parameters2. Springer Nature, Cham, pp. 63–150. https://doi.org/10.1007/978-3-031-11158-7_2.

Li, M., Neumayer, K.H., Flechtner, F., Lu, B., Förste, C., He, K., Xu, T., 2018. Performance assessment of multi-GNSS precise velocity and acceleration determination over Antarctica. J. Navig. 1–18. https://doi.org/10.1017/S0373463318000656.

Moorman, B.J., Michel, F.A., 1997. Bathymetric mapping and sub-bottom profiling through lake ice with ground-penetrating radar. J. Paleolimnol. https://doi.org/10.1023/A:1007920816271.

Nabighian, M.N., Ander, M.E., Grauch, V.J.S., Hansen, R.O., LaFehr, T.R., Li, Y., Pearson, W.C., Peirce, J.W., Phillips, J.D., Ruder, M.E., 2005. Historical development of the gravity method in exploration. Geophysics 70. https://doi.org/10.1190/1.2133785, 63ND-89ND.

Nixdorf, U., Steinhage, D., Meyer, U., Hempel, L., Jenett, M., Wachs, P., Miller, H., 1999. The newly developed airborne radio-echo sounding system of the AWI as a glaciological tool. Ann. Glaciol. 29, 231–238. https://doi.org/10.3189/172756499781821346.

Peshekhonov, V.A., Stepanov, O.A., Rozentsvein, V.G., Krasnov, A.A., Sokolov, A.V., 2022. State-of-the-art strapdown airborne gravimeters: analysis of the development. Gyrosc. A Navigat. 13, 3–35. https://doi.org/10.1134/S2075108722040101.

Petrovic, S., Barthelmes, F., Pflug, H., 2015. Airborne and shipborne gravimetry at GFZ with emphasis on the GEOHALO project. In: Rizos, C., Willis, P. (Eds.), International Association of Geodesy Symposia. Springer, Cham, pp. 313–322. https://doi.org/10.1007/1345_2015_17.

Scheinert, M., Ferraccioli, F., Schwabe, J., Bell, R., Studinger, M., Damaske, D., Jokat, W., Aleshkova, N., Jordan, T., Leitchenkov, G., Blankenship, D.D., Damiani, T.M., Young, D., Cochran, J.R., Richter, T.D., 2016. New Antarctic gravity anomaly grid for enhanced geodetic and geophysical studies in Antarctica. Geophys. Res. Lett. 43, 600–610. https://doi.org/10.1002/2015GL067439.

Simav, M., Becker, D., Yildiz, H., Hoß, M., 2020. Impact of temperature stabilization on the strapdown airborne gravimetry: a case study in Central Turkey. J. Geod. 94. https://doi.org/10.1007/s00190-020-01369-5.

Steinhage, D., 2001. Beiträge aus geophysikalischen Messungen in Dronning Maud Land, Antarktis, zur Auffindung eines optimalen Bohrpunktes für eine Eiskerntiefbohrung. Beiträge zur Polarforsch. 384, 1–91.

Studinger, M., Bell, R., Frearson, N., 2008. Comparison of AIRGrav and GT-1A airborne gravimeters for research applications. Geophysics 73. https://doi.org/10.1190/1.2969664.

Tankersley, M., 2023. Airborne Geophysical Investigation beneath Antarctica's Ross Ice Shelf. Victoria University of Wellington.

Vitushkin, L., Elinson, L.S., Krasnov, A.A., Peshekhonov, V.G., Sokolov, A.V., Smoller, Y., Yurist, S., 2022. Instruments for measuring gravity. In: Peshekhonov, V.G., Stepanov, O.A. (Eds.), Methods and Technologies for Measuring the Earth's Gravity Field Parameters. Springer Nature, Cham, pp. 1–61. https://doi.org/10.1007/978-3-031-11158-7_1.

Wei, M., Schwarz, K.P., 1998. Flight test results from a strapdown airborne gravity system. J. Geod. 323–332. https://doi.org/10.1007/s001900050171.

Wilson, J.P., 2012. Digital terrain modeling. Geomorphology 137, 107–121. https://doi.org/10.1016/j.geomorph.2011.03.012.

Yuan, Y., Gao, J., Wu, Z., Shen, Z., Wu, G., 2020. Performance estimate of some prototypes of inertial platform and strapdown marine gravimeters. Earth Planets Space 72, 1–11. https://doi.org/10.1186/s40623-020-01219-w.

Zhang, X., Zheng, K., Lu, C., Wan, J., Liu, Z., Ren, X., 2017. Acceleration estimation using a single GPS receiver for airborne scalar gravimetry. Adv. Sp. Res. 60, 2277–2288. https://doi.org/10.1016/j.asr.2017.08.038.

Zingerle, P., Pail, R., Gruber, T., Oikonomidou, X., 2019. The Experimental Gravity Field Model XGM2019e. https://doi.org/10.5880/ICGEM.2019.007.

Zingerle, P., Pail, R., Gruber, T., Oikonomidou, X., 2020. The combined global gravity field model XGM2019e. J. Geod. 94, 1–12. https://doi.org/10.1007/s00190-020-01398-0.